

Cite this: *Chem. Sci.*, 2011, **2**, 1262

www.rsc.org/chemicalscience

EDGE ARTICLE

Amorphous molybdenum sulfide films as catalysts for electrochemical hydrogen production in water†

Daniel Merki, Stéphane Fierro, Heron Vrubel and Xile Hu*

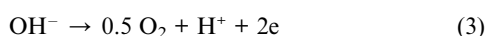
Received 28th February 2011, Accepted 25th March 2011

DOI: 10.1039/c1sc00117e

Amorphous molybdenum sulfide films are efficient hydrogen evolution catalysts in water. The films are prepared *via* simple electro-polymerization procedures and are characterized by XPS, electron microscopy and electronic absorption spectroscopy. Whereas the precatalysts could be MoS₃ or MoS₂, the active form of the catalysts is identified as amorphous MoS₂. Significant geometric current densities are achieved at low overpotentials (*e.g.*, 15 mA cm⁻² at $\eta = 200$ mV) using these catalysts. The catalysis is compatible with a wide range of pHs (*e.g.*, 0 to 13). The current efficiency for hydrogen production is quantitative. A 40 mV Tafel slope is observed, suggesting a rate-determining ion+atom step. The turnover frequency per active site is calculated. The amorphous molybdenum sulfide films are among the most active non-precious hydrogen evolution catalysts.

Introduction

Hydrogen is proposed as a major energy carrier for the future world.^{1,2} The most desirable source of hydrogen is water, as it is abundant and contains no carbon.¹ The production of hydrogen and oxygen from water, or “water splitting”, consists of two half cell reactions (eqn (1)–(3)).



The hydrogen evolution reaction (eqn (2)) requires catalysts. Whereas Ni based catalysts are often employed in commercial alkaline electrolyzers,³ Pt and its composites are the most active catalysts for hydrogen evolution in an acidic medium.⁴ Pt-type catalysts are more compatible with the conditions envisioned for photochemical water splitting, especially in direct photo-electrochemical approaches.⁵ However, the large scale application of Pt catalysts is limited by their high cost and low abundance. Extensive efforts have been devoted to the search of alternative catalysts containing only non-precious elements under heterogeneous conditions.^{6–10} Yet functional and robust catalysts operating with reasonable current densities (J) at low overpotentials (η) in water are scarce.^{7–10}

Recently, MoS₂ nanoparticles have been identified as promising hydrogen evolution catalysts. Bulk MoS₂ is a poor catalyst;¹¹ nano-crystals of MoS₂ and related metal sulfides, however, are more active.^{8,12,13} The best catalysts are crystalline, single-layered MoS₂ polygons deposited on Au(111), with $J \approx 0.2$ mA cm⁻² at $\eta = 150$ mV and pH = 0.⁸ Notwithstanding the impressive advances, the practical implementation of these systems is hindered by their sophisticated and/or energy intensive preparation procedures, such as ultra-high vacuum conditions, reduction by H₂S streams and annealing at elevated temperatures. Here we report that amorphous molybdenum sulfide films are active hydrogen evolution catalysts. The catalysts are prepared at room temperature and atmospheric pressure, and in a simple, rapid, and scalable manner. Furthermore, compared to MoS₂ nanoparticles, the amorphous molybdenum sulfide films exhibit higher activity.

Results and discussion

Deposition of MoS₃ film by cyclic voltammetry and characterization of this film

When studying the electrochemistry of [MoS₄]²⁻, we noticed that thin films were deposited onto the working electrodes by potential cycling experiments. For example, when the potential was cycled continuously from 0.3 V to -0.8 V vs. SHE (SHE = standard hydrogen electrode) at a rate of 50 mV s⁻¹ in a 2.0 mM aqueous solution of (NH₄)₂[MoS₄], one oxidation and one reduction peak grew in at -0.1 V and -0.6 V, respectively, concomitant with film formation (Fig. 1). After 5 scans, the film was visible; after 25 scans, the heights of the two redox peaks approached saturation. The deposition worked on different

Laboratory of Inorganic Synthesis and Catalysis, Institute of Chemical Sciences and Engineering, Ecole Polytechnique Fédérale de Lausanne (EPFL), EPFL-ISIC-LSCI, BCH 3305, Lausanne, CH 1015, Switzerland. E-mail: xile.hu@epfl.ch; Fax: +41 216939305; Tel: +41 216939781

† Electronic supplementary information (ESI) available: Experimental details and supplementary figures. See DOI: 10.1039/c1sc00117e

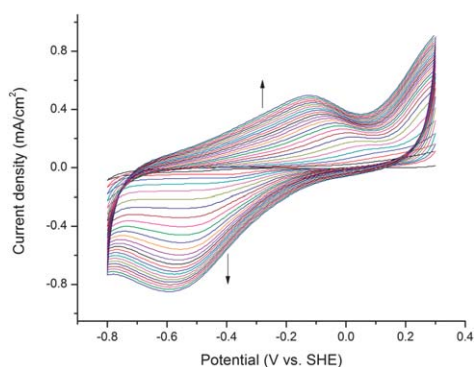


Fig. 1 Deposition of MoS₃-CV film on a FTO coated glass by repeated cyclic voltammetry (25 cycles) with a solution of [MoS₄]²⁻ in water. The arrows point to the growth of peaks during the deposition.

conducting substrates such as fluorine-doped tin oxide (FTO), indium tin oxide (ITO), and glassy carbon.

The X-ray photoelectron spectroscopy (XPS) survey spectrum of this film is dominated by the characteristic Mo and S peaks in addition to some smaller peaks of C and O from adventitious impurities (Fig. S2, ESI†). The binding energy of Mo 3d_{5/2} in the films is 228.6 eV, indicating a +4 oxidation state for the Mo ion (Fig. 2A).^{14,15} The S 2p spectrum (Fig. 2B) is best fit with two doublets, with S 2p_{3/2} energies of 162.4 and 163.9 eV, respectively. The spectrum indicates the presence of both S²⁻ and S₂²⁻ ligands.^{14,15} The spectrum is distinct from that of commercial MoS₂ particles (Fig S2, ESI†). Quantification by XPS gave a Mo/S ratio of 1 : 2.9. Both the Mo and S XPS spectra are similar to those of amorphous MoS₃,¹⁴ for which no hydrogen evolution activity was studied. Thus, we tentatively assign the material as MoS₃ (MoS₃-CV)¹⁶ with a formula of [Mo(IV)(S₂)²⁻]_{2.9}. There

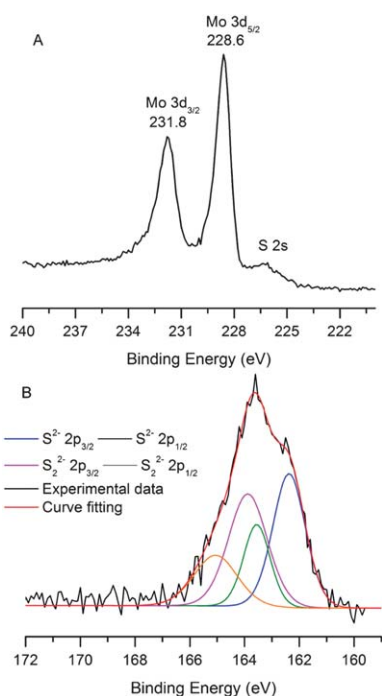


Fig. 2 XPS spectra of MoS₃-CV film on a FTO coated glass. (A) Mo 3d and S 1s region. (B) S 2p region.

might be some amount of amorphous MoS₂ whose XPS spectra is buried under those of MoS₃.

The formation of MoS₃-CV film from [MoS₄]²⁻ must result from an oxidation process. Bélanger *et al.* previously reported the electrodeposition of amorphous molybdenum sulfide from (NH₄)₂[MoS₄].¹⁷ It was shown that anodic electrolysis of an aqueous solution of (NH₄)₂[MoS₄] at *ca.* 0.55 V vs. SHE gave amorphous MoS₃ films which were identified by SEM,¹⁸ chemical analysis, XAS and XPS.¹⁹ The XPS data of those MoS₃ films resemble those in Fig. 2.

Fig. 3 shows typical transmission and scanning electron microscopy images of a film deposited on ITO. The film has a thickness of less than 100 nm, and is amorphous. No electron diffraction pattern was observed. The lack of crystallinity of the MoS₃-CV film is further confirmed by powder X-ray diffraction which shows no peak besides those from the tin oxide substrate (not shown).

It is possible to control the MoS₃-CV film thickness by the number of scan cycles and/or varying the concentration of the solutes (Fig. 4). Most films have a thickness between 40 and 150 nm. Increasing the number of scan cycles significantly increases the thickness, up until about 35 scan cycles. Then the thickness of the film approaches an upper limit (Fig. 4A). If deposited with the same number of scans (*e.g.*, 25), the film is thicker when the concentration of [MoS₄]²⁻ in the starting solution is higher.

Preparation and characterization of various MoS_x films

The MoS₃-CV film reported in this study is prepared by cyclic voltammetry at both anodic and cathodic potentials. While MoS₃ could be formed anodically (*vide supra*), amorphous MoS₂ film might be formed cathodically. Indeed, Lévy-Clément *et al.* reported that amorphous MoS₂ film was formed when an aqueous solution of (NH₄)₂[MoS₄] was electrolyzed at -0.75 to 1.15 V vs. SHE.²⁰ The MoS₂ film was X-ray amorphous, and electron probe microanalysis gave a S to Mo ratio of 1.9 to 2.1. Annealing of the

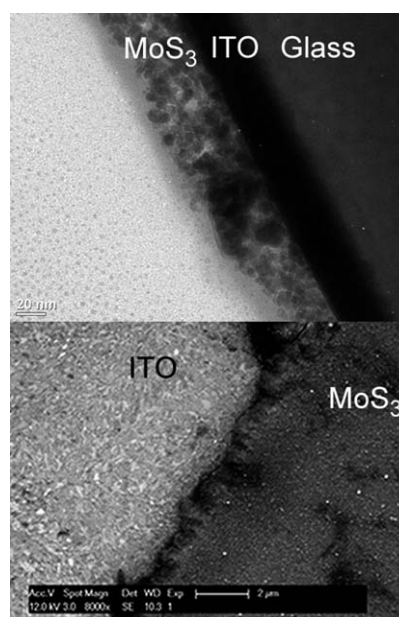


Fig. 3 Electron micrographs of the MoS₃-CV film on ITO.

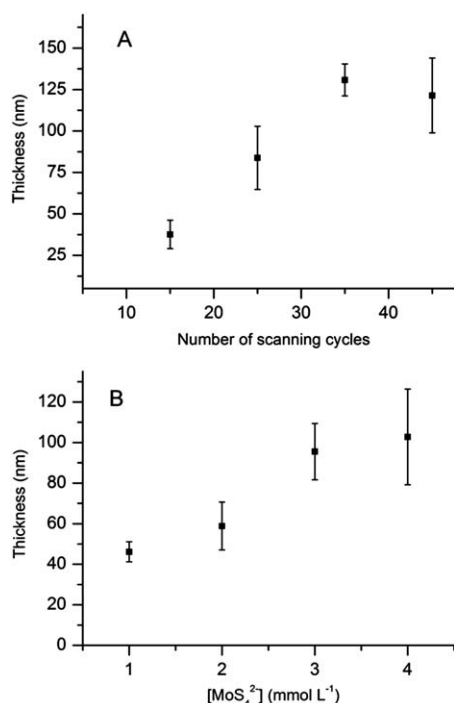


Fig. 4 Thickness of MoS₃-CV films on FTO as a function of scanning cycles and concentration of precursors. The measurements have been repeated multiple times to give the averaged values and error bars. (A) Thickness of MoS₃-CV films as a function of scanning cycles; the concentration of MoS₄²⁻ is 2.0 mM. (B) Thickness of MoS₃-CV films as a function of MoS₄²⁻ concentrations; 25 scanning cycles were applied for each deposition.

MoS₂ at 550 °C in Ar then gave the crystalline MoS₂ particles.²⁰ Judging from the potential window of our cyclic voltammetric experiments in Fig. 1, we suspected that a small amount of amorphous MoS₂ was also produced together with MoS₃ in the MoS₃-CV film. To evaluate the catalytic property of different amorphous MoS_x films, we decided to prepare MoS₃ and MoS₂ films according to the methods of Bélanger and Lévy-Clément. Furthermore, we also prepared a molybdenum sulfide film by the same continuous cyclic voltammetry as in Fig. 1, with the exception that the scans started from -0.8 to 0.3 V, and the final scan finished at -0.8 V. This way, the formation of film was terminated at the cathodic potential.

XPS was used to identify the chemical compositions of these new films. The XPS spectra of MoS₃ film prepared by the method of Bélanger (MoS₃-AE, Fig. S3, ESI†)¹⁶ are very similar to those in Fig. 2. The S to Mo ratio is 3.2. The XPS spectra of MoS₂ film (MoS₂-CE, Fig. S3, ESI†)¹⁶ prepared by the method of Lévy-Clément are similar to those of commercial MoS₂ particles, and do not contain the S peaks from S₂²⁻. The S to Mo ratio is 1.9. Interestingly, the molybdenum sulfide film prepared by cyclic voltammetry finishing at the cathodic potential gives XPS spectra similar to the MoS₂ film and MoS₂ particles (Fig. S3, ESI†). The S to Mo ratio is 2. We assign this film to MoS₂-CV,¹⁶ although it probably contains a small amount of MoS₃ that cannot be detected by XPS in the presence of a large amount of MoS₂.

In addition to XPS, UV-Vis absorption spectroscopy was used to characterize the four different types of MoS_x films. The films exhibit similar spectra with absorption peaks at ca. 310, 375, 480,

and 630 nm (Fig. S4, ESI†), probably because they all contain Mo(IV) ions and S²⁻ ligands. No absorption peaks associated with the S₂²⁻ ligands in MoS₃-CV and MoS₃-AE films could be located.

Hydrogen evolution activity of four MoS_x films

The catalytic activity of the four MoS_x films was studied by electrochemistry. Fig. 5 shows the polarization curves of MoS₃-CV on a rotating glassy carbon disk electrode at pH = 0 to 5; Fig. S5, ESI† shows its polarization curves at pH = 7, 9, 11, 13, and the curve for MoS₃-CV deposited on FTO at pH = 2. The MoS₃-CV films display high catalytic activity for hydrogen evolution at a wide range of pH values. As expected, the apparent current densities decrease with an increase of pHs (Fig. S5, ESI†). At low overpotentials ($\eta < 250$ mV), the current is independent of rotating rates and therefore kinetic-controlled. The amorphous MoS₃-CV is more active than the MoS₂ single crystals deposited on Au(111).⁸ The apparent current density (J) for the MoS₃-CV film at $\eta = 150$ mV is ca. 0.4 mA cm⁻² at pH = 0, higher than that for the MoS₂ crystals at the same overpotential ($J \approx 0.2$ mA cm⁻²).

The catalytic activity of MoS₃-AE film is nearly identical to that of MoS₃-CV film (Fig. 6), except that the activity decreases gradually during consecutive scans (Fig. S6, ESI†). In contrast, the activity of MoS₃-CV film remains constant during consecutive scans (Fig. S6, ESI†). The higher stability of MoS₃-CV film compared to MoS₃-AE film suggests an advantage for the potential-cycling process.

Interestingly, the MoS₂-CV film, made also through the potential-cycling process, is as active and stable as the MoS₃-CV film (Fig. 6 and Fig. S6, ESI†). This observation raised the question: what is the active catalyst for all the amorphous MoS_x films? It prompted us to study the MoS_x films after catalysis (*vide infra*). The MoS₂-CE film, prepared by potentiostatic cathodic electrolysis, is the least active catalyst (Fig. 6). Its activity also decreases during consecutive scans (Fig. S6, ESI†).

Active catalyst

All four MoS_x films exhibited hydrogen evolution activity. These films are better considered as pre-catalysts. To verify if these pre-catalysts were activated to form the same catalyst under the

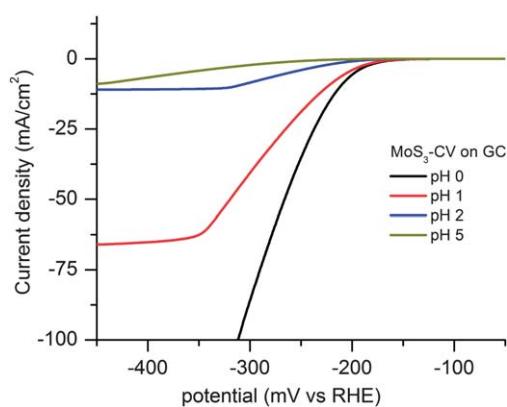


Fig. 5 Polarization curves of MoS₃-CV film on a rotating glassy carbon disk electrode recorded at pH = 0, 1, 2, and 5. Scan rate: 2 mV s⁻¹; rotating rate: 4500 rpm.

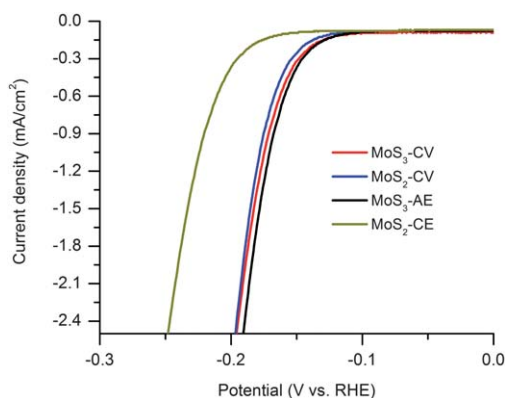


Fig. 6 Polarization curves of MoS_x -films on FTO recorded at $\text{pH} = 0$. Scan rate: 2 mV s^{-1} . The curves are from the second polarization scans for the freshly prepared samples, some of which need a pre-activation process in the first polarization scan (see main text for details).

conditions for hydrogen evolution, we carefully examined the first polarization curves for the freshly prepared films. Indeed a pre-activation process was found for MoS_3 -CV, MoS_3 -AE, MoS_2 -CV, but not for MoS_2 -CE.

For MoS_3 -CV and MoS_3 -AE, a reduction peak was observed prior to hydrogen evolution (Fig. 7). The same reduction peak was observed for MoS_2 -CV, but it was significantly smaller. No reduction was observed for MoS_2 -CE. For all MoS_x films, no reduction peak before hydrogen evolution was observed in the second and following polarization scans (Fig. 6).

We hypothesized that the reduction peak in the first scan originated from the reduction of MoS_3 to MoS_2 , whereby the S_2^{2-} accepted two electrons to form S^{2-} . The MoS_2 species is then responsible for the hydrogen evolution catalysis. To verify this hypothesis, we carried out a XPS study on the MoS_3 -CV film after several polarization measurements. The XPS spectra of the film have changed, and are similar to those of MoS_2 (Fig. S7, ESI†). The peaks of S_2^{2-} disappeared. We recognize that XPS is a surface technique, and plan to carry out a similar study using a technique that can probe the bulk composition of the thin films, e.g., XAS.

The UV-Vis spectra of the four MoS_x films after multiple polarization scans were measured and are similar. They are also similar to the spectra of freshly prepared samples (Fig. S8, ESI†). While the UV-Vis spectra of these films are not sensitive to the

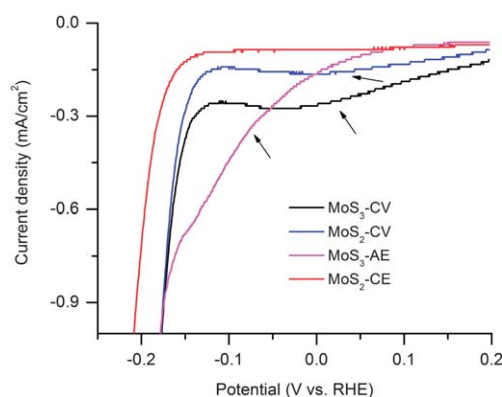


Fig. 7 First polarization curves of freshly prepared MoS_x films on FTO at $\text{pH} = 0$. The arrows point to the reduction prior to hydrogen evolution.

presence or absence of S_2^{2-} ligand, they suggest that the bulk compositions of the films are MoS_x , and most likely MoS_2 .

It thus appears that amorphous MoS_2 is the real catalyst for all four MoS_x films. The MoS_3 -CV and MoS_2 -CV films reported here are the best precatalysts in terms of activity and stability and they are indistinguishable. The MoS_3 -AE film is as active, but some MoS_3 in this film might be re-dissolved at cathodic potentials to form the soluble species $[\text{MoS}_4]^{2-}$. For this reason it loses activity during consecutive scans. This problem is alleviated in the potential cycling procedures used to make the MoS_3 -CV and MoS_2 -CV films. The MoS_2 -CE film is the least active and least stable catalyst. We suspect that when deposited at a very negative potentials, the film is more rapidly formed and is structurally inferior.

Only MoS_3 -CV film is used for the further studies in this paper.

Tafel analysis and bulk electrolysis

Tafel behavior was observed for the polarization curve of MoS_3 -CV on glassy carbon at $\eta = 120$ to 200 mV and $\text{pH} = 0$ (Fig. 8). Analysis of the data at $\eta = 170$ to 200 mV gave a Tafel slope of 40 mV per decade and an apparent J_0 of ca. $1.3 \times 10^{-7} \text{ A cm}^{-2}$ for a film made from 25 scanning cycles (Fig. S9, ESI†).

Bulk electrolysis was carried out to determine the current efficiency of hydrogen evolution. In a 1 M solution of H_2SO_4 , the MoS_3 -CV film deposited on a glassy carbon disk (25 cycles) gave current densities of 160 and 14 mA cm^{-2} at $\eta = 300$ and 200 mV , respectively. These current densities are among the highest reported for non-noble catalysts in acidic or neutral conditions.^{10,21} For comparison, a recently reported and very active Ni-bisphosphine/carbon nanotube based H_2 production catalyst gave a current density of 20 mA cm^{-2} at $\eta = 300 \text{ mV}$.⁹ The Faraday yields for H_2 production were found to be quantitative within experimental errors. By measuring pressure change during water splitting, it was possible to monitor H_2 production *in situ*. Fig. 9 and Fig. S10, ESI† show that the current efficiency remains quantitative for hours. Thus, while it was reported that vacuum-dried MoS_3 could absorb H_2 to form H_2S ,²² under the electrolysis conditions, the MoS_3 -CV film reported here remains stable and active during H_2 production.

The catalytic activity of the MoS_3 -CV films depends on the thickness. Fig. 10A shows the polarization curves of films deposited on a rotating glassy carbon electrode with different

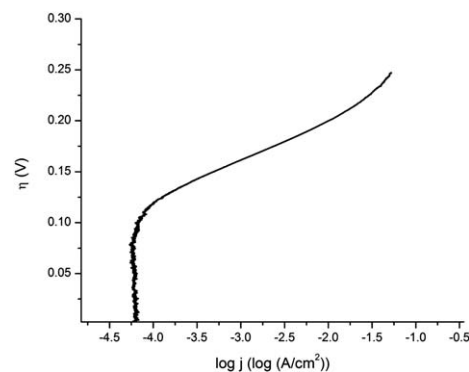


Fig. 8 Tafel plot of the polarization curve of MoS_3 -CV film on glassy carbon at $\text{pH} = 0$. The film was made with 25 scanning cycles. Scan rate for polarization: 1 mV s^{-1} .

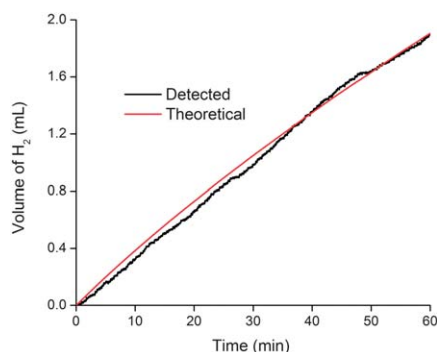


Fig. 9 Current efficiency for H_2 production catalyzed by a MoS_3 -CV film on glassy carbon at $\text{pH} = 0$ and 200 mV overpotential. The theoretical line was calculated according to the cumulative charge, assuming a 100% Faraday's yield for H_2 production. The current density was *ca.* 14 mA cm^{-2} .

scanning cycles. Films deposited by higher numbers of cycles are more active. The intrinsic catalytic activity is however measured by the turnover frequency (TOF) for each active site. We attempted to quantify the active sites by electrochemistry. Fig. 10B shows the cyclic voltammograms in the region of -0.2 V to 0.6 V vs. RHE for the MoS_3 -CV films at $\text{pH} = 7$. While it is difficult to assign the observed peaks to a given redox couple, the integrated charge over the whole potential range should be proportional to the total number of active sites. Assuming a one-electron process for both reduction and oxidation, the upper limit of active MoS_2 sites could be calculated for each film. Fig. 10C shows the polarization curves at $\text{pH} = 0$ normalized by the active sites, and expressed in terms of TOF (see ESI†). Up to $\eta = 200 \text{ mV}$, a fairly uniform activity was observed for films made from different scan cycles, suggesting that even though there is a significant uncertainty in the estimation of the active sites, self-consistent information on the site-averaged catalytic activity can be extracted from this analysis. At $\eta > 200 \text{ mV}$, some deviations were observed, probably due to the influence of substrate diffusion. Fig. S11, ESI,† shows the calculated TOFs at $\text{pH} = 7$.

The rough estimation of TOFs makes it possible to compare the activity of MoS_3 -CV film with other catalysts. The most active catalyst, Pt, has a TOF of 0.8 s^{-1} at $\eta = 0$ and $\text{pH} = 0$,⁸ to reach the same TOF, MoS_3 -CV films need an overpotential of *ca.* 220 mV. An interesting Mo-oxo system is reported to work on a mercury pool electrode on which it might be adsorbed.²³ It has a TOF of 2 s^{-1} at $\eta \approx 1000 \text{ mV}$ at $\text{pH} = 7$. The TOF of MoS_3 -CV film reaches the same value at $\eta \approx 240 \text{ mV}$ and $\text{pH} = 0$. The Mo-oxo system uses water as the substrate, while the MoS_3 -CV system uses protons as the substrate. To make a fair comparison, we also measured the TOFs of a MoS_3 -CV film at $\text{pH} = 7$ (Fig. S11, ESI†). The Mo-oxo system has a TOF of 0.3 s^{-1} at $\eta \approx 600 \text{ mV}$,²³ while the MoS_3 -CV film reaches the same TOF at $\eta \approx 340 \text{ mV}$. Thus, amorphous MoS_3 -CV compares favorably with known non-precious catalysts in terms of bulk catalytic properties.

Mechanism of hydrogen evolution

Given that single crystals and nanoparticles of MoS_2 but not bulk MoS_2 are active H_2 evolution catalysts, the discovery that the four amorphous MoS_x films are active catalysts was

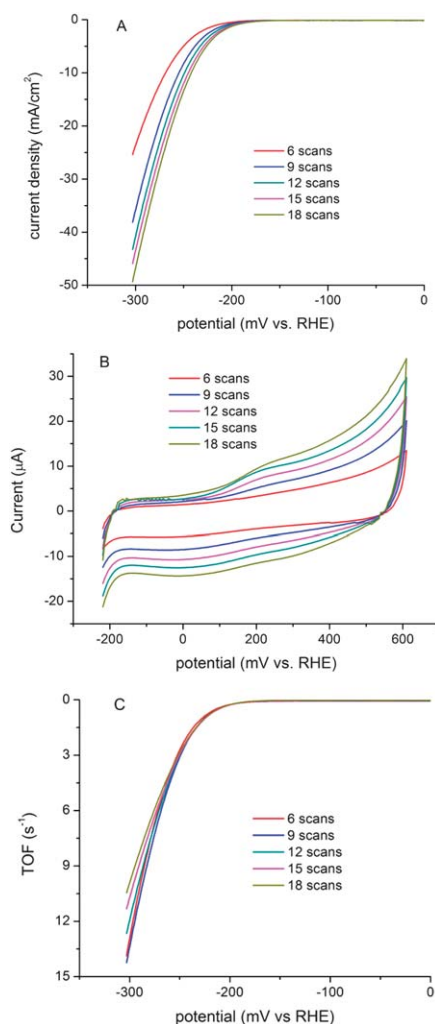
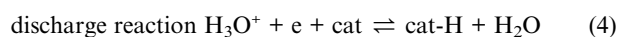


Fig. 10 (A) Polarization curves of MoS_3 -CV films made from different numbers of scanning cycles recorded at $\text{pH} = 0$. The films were deposited on a rotating glassy carbon electrode. Scan rate: 1 mV s^{-1} ; rotating rate: 2000 rpm. (B) Cyclic voltammograms of the same MoS_3 -CV films recorded at $\text{pH} = 7$ and between -0.2 V and 0.6 V vs. RHE; scan rate: 50 mV s^{-1} . (C) Calculated turnover frequencies for the MoS_3 -CV films at $\text{pH} = 0$.

unexpected. The overall catalytic activity per geometric area of MoS_3 -CV and MoS_2 -CV film is higher than that of MoS_2 single crystals (*vide infra*) and nanoparticles ($J \approx 160 \text{ mA cm}^{-2}$ at $\eta \approx 300 \text{ mV}$ for MoS_3 -CV film and $J < 2 \text{ mA cm}^{-2}$ at $\eta \approx 300 \text{ mV}$ for MoS_2 nanoparticles).¹³

H_2 evolution by amorphous MoS_2 (which is the active species in all four MoS_x films) seems to proceed *via* a different mechanism from that by MoS_2 single crystals and nanoparticles. MoS_2 films have a Tafel slope of 40 mV per decade. This Tafel slope is different from those of MoS_2 crystals⁸ (55 to 60 mV per decade) or MoS_2 nanoparticulate¹³ (120 mV per decade). According to the classic theory on the mechanism of hydrogen evolution,²⁴ a Tafel slope of 40 mV indicates that the surface coverage of adsorbed hydrogen is less than 10%, and hydrogen production occurs *via* a fast discharge reaction (eqn (4)) and then a rate-determining ion+atom reaction (eqn (5)).



ion + atom reaction $\text{H}_3\text{O}^+ + \text{e} + \text{cat-H} \rightleftharpoons \text{cat} + \text{H}_2 + \text{H}_2\text{O}$ (5)

combination reaction $\text{cat-H} + \text{cat-H} \rightleftharpoons 2\text{cat} + \text{H}_2$ (6)

A Tafel slope of 60 mV per decade indicates a larger surface coverage of adsorbed hydrogen and a rate-determining recombination (eqn (6)) or ion+atom reaction.²⁵ A Tafel slope of 120 mV could arise from various reaction pathways depending on the surface coverage.²⁴ The different Tafel slopes point to a unique catalytic property for amorphous MoS_x films when compared to crystalline forms of MoS_2 . For MoS_2 single crystals and nanoparticles, the active sites are proposed to be on the edges which have coordinatively unsaturated Mo and/or S atoms.⁸ The MoS_2 films described here may have more such unsaturated sites thanks to their amorphous nature. We suspect that this is the reason why the films are more active than the single crystals and nanoparticles. More work is required to shed light on the mechanism of H_2 evolution at the molecular level. Given that both Mo and S are capable of accepting electrons and protons, a ‘bifunctional’, metal–ligand cooperative mode of catalysis is probable.²⁶

Conclusions

In summary, we show that amorphous MoS_x films are highly active hydrogen evolution catalysts. While the precatalysts can exist in various forms of molybdenum sulfide, the real catalyst is amorphous MoS_2 . The catalyst is made of relatively cheap and abundant elements and offers significant advantages over noble metal catalysts. The catalyst can be easily prepared in a procedure that is amenable to large scale manufacture. The catalyst works in water and is compatible with a wide range of pHs. Significant current densities could be obtained at low overpotentials and the current efficiency for H_2 production is quantitative. Our results thus provide new opportunities for the development of renewable and economic hydrogen production technologies. Further characterization and application of the catalyst, such as further stability studies and impedance analysis are currently underway.

Acknowledgements

This work is supported by the EPFL, the Swiss National Science Foundation (project number 200021_119663), and a starting grant from the European Research Council under the European Community’s Seventh Framework Programme (FP7 2007–2013)/ERC Grant agreement n° 257096. X.L. Hu thank Prof. Nathan Lewis (Caltech) and Profs. Michael Grätzel, Hubert Girault and Christos Comninellis (EPFL) for discussion and suggestions. Nicolas Xanthopoulos is acknowledged for help with XPS measurements.

Notes and references

1 J. A. Turner, *Science*, 2004, **305**, 972–974.

- N. S. Lewis and D. G. Nocera, *Proc. Natl. Acad. Sci. U. S. A.*, 2006, **103**, 15729–15735.
- J. Ivy *Summary of electrolytic hydrogen production*. Milestone completion report NREL/MP-560–36734. National Renewable Energy Laboratory: Golden, Colorado; 2004; G. Schiller, R. Henne, P. Mohr and V. Peinecke, *Int. J. Hydrogen Energy*, 1998, **23**, 761–765.
- D. E. Bartak, B. Kazee, K. Shimazu and T. Kuwana, *Anal. Chem.*, 1986, **58**, 2756–2761; P. Millet, F. Andolfatto and R. Durand, *Int. J. Hydrogen Energy*, 1996, **21**, 87–93.
- H. B. Gray, *Nat. Chem.*, 2009, **1**, 7–7; W. J. Youngblood, S. H. A. Lee, K. Maeda and T. E. Mallouk, *Acc. Chem. Res.*, 2009, **42**, 1966–1973.
- F. A. Armstrong, N. A. Belsey, J. A. Cracknell, G. Goldet, A. Parkin, E. Reisner, K. A. Vincent and A. F. Wait, *Chem. Soc. Rev.*, 2009, **38**, 36–51; M. M. Jaksic, *Electrochim. Acta*, 2000, **45**, 4085–4099.
- L. A. Berben and J. C. Peters, *Chem. Commun.*, 2010, **46**, 398–400; B. Keita and L. Nadjo, *J. Electroanal. Chem.*, 1985, **191**, 441–448; B. Keita and L. Nadjo, *Mater. Chem. Phys.*, 1989, **22**, 77–103; B. Winther-Jensen, K. Fraser, C. Ong, M. Forsyth and D. R. MacFarlane, *Adv. Mater.*, 2010, **22**, 1727–1730.
- T. F. Jaramillo, K. P. Jorgensen, J. Bonde, J. H. Nielsen, S. Horch and I. Chorkendorff, *Science*, 2007, **317**, 100–102.
- A. Le Goff, V. Artero, B. Jusselme, P. D. Tran, N. Guillet, R. Metaye, A. Fihri, S. Palacin and M. Fontecave, *Science*, 2009, **326**, 1384–1387; P. D. Tran, A. Le Goff, H.J., B. Jusselme, N. Guillet, S. Palacin, H. Dau, M. Fontecave and V. Artero, *Angew. Chem., Int. Ed.*, 2011, **50**, 1371–1374.
- E. Navarro-Flores, Z. W. Chong and S. Omanovic, *J. Mol. Catal. A: Chem.*, 2005, **226**, 179–197.
- W. Jaegermann and H. Tributsch, *Prog. Surf. Sci.*, 1988, **29**, 1–167.
- B. Hinnemann, P. G. Moses, J. Bonde, K. P. Jorgensen, J. H. Nielsen, S. Horch, I. Chorkendorff and J. K. Nørskov, *J. Am. Chem. Soc.*, 2005, **127**, 5308–5309; X. Zong, H. J. Yan, G. P. Wu, G. J. Ma, F. Y. Wen, L. Wang and C. Li, *J. Am. Chem. Soc.*, 2008, **130**, 7176–7177.
- J. Bonde, P. G. Moses, T. F. Jaramillo, J. K. Nørskov and I. Chorkendorff, *Faraday Discuss.*, 2009, **140**, 219–231.
- T. Weber, J. C. Muijsers and J. W. Niemantsverdriet, *J. Phys. Chem.*, 1995, **99**, 9194–9200.
- J. C. Muijsers, T. Weber, R. M. vanHardeveld, H. W. Zandbergen and J. W. Niemantsverdriet, *J. Catal.*, 1995, **157**, 698–705.
- In this paper, we abbreviate the films by their preparative methods. CV designates the films made by cyclic voltammetry, AE designates the films made by anodic electrolysis and CE designates the films made by cathodic electrolysis.
- G. Laperriere, B. Marsan and D. Belanger, *Synth. Met.*, 1989, **29**, 201–F206.
- D. Belanger, G. Laperriere and B. Marsan, *J. Electroanal. Chem.*, 1993, **347**, 165–183.
- D. Belanger, G. Laperriere, F. Girard, D. Guay and G. Tourillon, *Chem. Mater.*, 1993, **5**, 861–868.
- E. A. Ponomarev, M. Neumann-Spallart, G. Hodes and C. Levy-Clement, *Thin Solid Films*, 1996, **280**, 86–89.
- NiMo alloys were reported to have similar activity, but largely due to the high surface roughness. The normalized geometric current density is ca. 0.015 mA cm⁻² at $\eta = 150$ mV, smaller than 0.4 mA cm⁻² found for the MoS_3 -CV film. See ref. 10.
- P. Afanasiev, H. Jobic, C. Lorentz, P. Leverd, N. Mastubayashi, L. Piccolo and M. Vrinat, *J. Phys. Chem. C*, 2009, **113**, 4139–4146.
- H. I. Karunadasa, C. J. Chang and J. R. Long, *Nature*, 2010, **464**, 1329–1333.
- J. O. M. Bockris and E. C. Potter, *J. Electrochem. Soc.*, 1952, **99**, 169–186.
- J. G. Thomas, *Trans. Faraday Soc.*, 1961, **57**, 1603–1611.
- M. R. DuBois and D. L. DuBois, *Chem. Soc. Rev.*, 2009, **38**, 62–72; A. M. Appel, D. L. DuBois and M. R. DuBois, *J. Am. Chem. Soc.*, 2005, **127**, 12717–12726; T. B. Rauchfuss, *Inorg. Chem.*, 2004, **43**, 14–26.